RESEARCH PAPER

Synthesis Characterization of Chalcone, Coumarin Based Novel Heterocyclic Polymer for Antibacterial Activity

Rusvi A. Gandhi[1], Umesh P. Tarpada[2*], Vivek N. Dave[3], Kaushik N. Kundaliya[4], Dilip V. Vasava[5]

[1] Research Scholar, Department of Chemistry, Gujarat University, Ahmedabad, Gujarat, India

[2-4] Department of Chemistry, Government Arts & Science College, Bavla, Gujarat University, Ahmedabad, Gujarat, India

[5] Department of Chemistry, Gujarat University, Ahmedabad, Gujarat, India

[*] Email: umeshtarpada@gmail.com

Received: 12th Mar, 2026 | **Revised:** 24th Mar, 2026 | **Accepted:** 14th Apr, 2026 | **Available Online:** 30th Apr, 2026

ABSTRACT

This study addresses the urgent need for innovative antibacterial agents due to the rise of multidrug-resistant bacteria. Heterocyclic polymers functionalized with chalcone and coumarin moieties were synthesized and characterized using FTIR and NMR (^{1}H and ^{13}C) spectroscopy, confirming the presence of key functional groups like carbonyl, triazole, and aromatic rings critical for antibacterial activity. The antibacterial efficacy of five synthesized compounds (8a–8e) was tested against Gram-positive (Staphylococcus aureus, Bacillus megaterium) and Gram-negative (Escherichia coli, Proteus vulgaris) bacteria. Compound 7b showed notable activity, with inhibition rates of up to 63.1% against S. aureus and 57.0% against E. coli. Compound 7e exhibited the highest efficacy, achieving over 81% inhibition against S. aureus and B. megaterium. Compound 8b demonstrated comparable efficacy to Ampicillin, achieving 0.6-fold activity relative to the antibiotic. The enhanced antibacterial properties were attributed to the synergistic action of chalcone and coumarin moieties, which disrupt bacterial membranes, inhibit vital enzymes, and induce oxidative stress. With high bioavailability, stability, and low cytotoxicity, these polymers show promise for biomedical applications.

Keyword: Chalcone, Coumarin, Antibacterial Activity, Multidrug Resistance, Polymer Synthesis

How to cite this article: Gandhi RA, Tarpada UP, Dave VN, Kundaliya KN, Vasava DV. Synthesis Characterization of Chalcone, Coumarin Based Novel Heterocyclic Polymer for Antibacterial Activity. Int J Drug Deliv Technol. 2026;16(39s): 933-944. DOI: 10.25258/ijddt.16.39s.127

Source of support: Nil.

Conflict of interest: None

Introduction

The rapid rise of multidrug-resistant bacterial strains has intensified the search for new antibacterial agents, with heterocyclic polymers emerging as promising candidates due to their notable efficacy [1–5]. Heterocyclic compounds are organic molecules containing one or more heteroatoms within cyclic or acyclic frameworks [6–10]. Their antibacterial activity arises from mechanisms such as disruption of bacterial membranes [11], interference with metabolic pathways [12], and generation of reactive oxygen species [13]. Moreover, their tuneable chemical structures allow optimization of bioavailability, selectivity, and biodegradability, enhancing their pharmaceutical relevance [14], [15].

Heterocyclic polymers incorporating bioactive moieties such as chalcones and coumarins represent a novel class of antibacterial materials [16]. These polymers, containing heteroatoms like nitrogen, oxygen, or sulfur within their backbone, exhibit enhanced physicochemical stability and biological performance [17]. Structural versatility enables the incorporation of diverse functional groups, significantly improving antibacterial activity [18–21]. Combined with their biocompatibility, these properties position heterocyclic polymers as effective tools against antimicrobial resistance [22], [23].Coumarins have received considerable attention due to their wide range of pharmacological activities, including antidepressant [24], antimicrobial [25], antioxidant [26], anti-inflammatory [27], and antinociceptive effects [28]. Chalcones, a class of α,β-unsaturated ketones, are well known for strong antimicrobial activity mediated through membrane disruption, enzyme inhibition, and metabolic interference [8], [29–32]. Incorporation of chalcones into polymeric systems enhances both antibacterial efficacy and structural integrity. Similarly, coumarins exhibit antibacterial

effects by targeting DNA gyrase, inducing oxidative stress, and destabilizing bacterial membranes. Their integration into heterocyclic polymers improves solubility, biodegradability, and biocompatibility.

The combined incorporation of chalcone and coumarin units within a heterocyclic polymer framework offers a synergistic antibacterial effect. Their complementary mechanisms enhance interaction with bacterial cell walls, disrupt essential cellular processes, and help overcome resistance mechanisms. This dual-functionalization strategy results in materials effective against both Gram-positive and Gram-negative bacteria, with improved resistance to enzymatic degradation and low cytotoxicity. In this study, we report the synthesis and antibacterial evaluation of heterocyclic polymers functionalized with chalcone and coumarin derivatives. The polymers were designed to enhance membrane interaction, inhibit key bacterial enzymes, and induce oxidative stress while maintaining structural stability and targeted bioactivity. This work provides valuable insights into the rational design of bioactive heterocyclic polymers and highlights their potential as next-generation antibacterial materials.

Result and Discussion

Synthesis and Characterization: The synthesis of the final heterocyclic polymer hybrid compound was meticulously executed through a strategically designed multistep synthetic protocol, explicitly tailored to ensure maximum efficiency, scalability, and yield. This well-defined sequence of chemical transformations, systematically optimized for each step, is comprehensively illustrated in **Scheme 1-4**. Initially, Compound 1 was obtained via aldol condensation between a methoxy-substituted aromatic compound and hydroxybenzaldehyde in ethanol under basic conditions using sodium hydroxide as a catalyst. The reaction yielded a crystalline chalcone derivative after neutralization and recrystallization. Compound 3 was subsequently synthesized through a condensation reaction between Compound 1 and a hydrazine derivative in glacial acetic acid. The reaction proceeded smoothly at room temperature, as monitored by TLC, and the product was purified using column chromatography to ensure high purity.

Compound 4 was prepared by reacting Compound 3 with propargyl bromide in dry acetone under reflux conditions, with potassium carbonate acting as the base. This step produced the propargyl derivative with excellent yield and selectivity, facilitated by effective removal of inorganic salts and subsequent purification. In a parallel step, Compound 6 was synthesized via substitution of dibromo alkane with sodium azide in ethanol. The reaction proceeded efficiently under reflux, resulting in complete conversion to the azide derivative within 6 hours, as confirmed by TLC.

Finally, the Cu(I)-catalyzed azide-alkyne cycloaddition (CuAAC) reaction, a well-established "click chemistry" approach, was employed to couple Compounds 4 and 6. This reaction was carried out in dry DMF at room temperature using potassium carbonate and copper(I) iodide as the catalytic system. The reaction conditions facilitated the selective formation of the triazole-linked final product, which was subsequently purified by column chromatography to achieve high purity. This synthetic pathway represents a robust and reproducible approach for the preparation of structurally diverse derivatives, offering significant potential for further applications.

This **table 1** summarizes the influence of various reaction conditions on the yield of a process catalyzed by CuI. The molar percentage of CuI, ranging from 0.05% to 1%, plays a critical role in optimizing the reaction efficiency, with the highest yield (92%) observed at 1% CuI, particularly in DMF at 100°C for 6 hours, using KOH as the base.Solvent choice is another key factor. Polar solvents like DMF and DMSO, used at higher temperatures (100-120°C), tend to enhance the solubility of reactants and facilitate better reaction kinetics, resulting in higher yields (92% and 82% respectively in DMF). In contrast, non-polar solvents like toluene and ethanol yielded lower results, likely due to their poorer ability to dissolve reactants and lower reactivity under the same conditions.

The reaction temperature also plays a significant role. Higher temperatures (100°C to 120°C) generally lead to higher yields, but this is contingent on the solvent's ability to support such temperatures without causing side reactions or decomposition. Reaction time, ranging from 4 to 12 hours, seems to contribute to achieving higher yields, though excess time does not always correlate with a substantial increase in yield.The base used in the reaction affects both the reaction rate and the overall efficiency. Bases KOH and K_2CO_3 resulted in higher yields compared to bases like NaOH and Et_3N, suggesting that stronger or more reactive bases may be more effective in promoting the desired reaction. Overall, based on data we finding CuI concentration, solvent polarity, reaction temperature, base selection, and reaction time in determining the success of the process. Fine-tuning these parameters is crucial for optimizing reaction conditions and maximizing yield.

The ^{1}H NMR spectrum of **compound 1** (3,4-dihydroxychalcone) shows peaks for aromatic protons in the region of **δ ~ 6.8–8.0 ppm**, with splitting patterns

reflecting the substituted benzene rings. The protons on the electron-rich aromatic ring (with hydroxyl groups) appear at **δ ~ 6.8–7.5 ppm**, while the protons on the carbonyl-substituted ring resonate at **δ ~ 7.5–8.0 ppm**. The olefinic protons from the α, β-unsaturated ketone contributes to signals around **δ ~ 7.5 ppm**. A broad peak at **δ ~ 9.0 ppm** corresponds to the hydroxyl (-OH) protons, which are downfield due to hydrogen bonding. The ^{1}H NMR spectrum of **compound 3** shows aromatic protons as multiplets in the range of **δ 6.5–8.0 ppm**, corresponding to the protons on the three benzene rings, influenced by the hydroxyl (-OH) groups and the azo (-N=N-) linkage. The hydroxyl protons (-OH) appear as broad peaks around **δ 9.0–10.0 ppm**, deshielded due to hydrogen bonding. This pattern aligns with the molecule's structure, confirming the presence of substituted aromatic systems. The ^{1}HNMR spectrum of **compound 5** show peaks corresponding to the aromatic protons on the coumarin ring system in the range of **δ 7.0–8.5 ppm**, influenced by the electron-withdrawing nitro group (-NO_2). The methylene (-CH_2-) protons in the brominated alkyl chain are expected to appear as triplets or multiplets around **δ 3.5–4.5 ppm** due to their proximity to the electronegative oxygen and bromine atoms. The terminal methylene (-CH_2-Br) protons are further deshielded and resonate at **δ 3.0–3.5 ppm**. The FTIR spectrum of **7a** exhibits characteristic bands corresponding to its diverse functional groups. A strong absorption band around **1700–1750 cm^{-1}** is indicative of the stretching vibrations of carbonyl (C=O) groups from the coumarin moieties. The nitro (-NO_2) groups display prominent asymmetric and symmetric stretching vibrations at **1500–1550 cm^{-1}** and **1300–1350 cm^{-1}**, respectively. The aromatic rings contribute C=C stretching bands in the range of **1450–1600 cm^{-1}**, while C-N stretching vibrations from the triazole linkages are observed around **1200–1350 cm^{-1}**. The ether linkages (-C-O-C-) exhibit stretching bands near **1050–1150 cm^{-1}**, and the aliphatic methylene (-CH_2-) groups show C-H stretching in the region of **2850–2950 cm^{-1}**. Additionally, aromatic C-H stretching vibrations appear near **3000–3100 cm^{-1}**. These features collectively confirm the presence of carbonyl, nitro, aromatic, triazole, and ether functional groups in the compound. In the ^{1}HNMR spectrum of compound **7a**, aromatic protons resonate in the range of **δ 6.5–8.5 ppm**, with distinct multiplets due to the various substituents and electronic environments around the aromatic systems. The methylene (-CH_2-) protons bridging the triazole and coumarin units appear in the region of **δ 3.5–5.5 ppm**, exhibiting splitting patterns consistent with adjacent electronegative groups. The peaks around **δ 2.0–3.0 ppm** correspond to alkyl protons connected to electron-withdrawing nitro and oxygen groups also, ^{13}C spectrum observed the signals between **δ 110–160 ppm** correspond to aromatic carbons from the coumarin, nitrobenzene, and triazole systems. Peaks around **δ 150–160 ppm** are attributed to quaternary carbons bonded to electron-withdrawing groups, such as carbonyl (C=O). The coumarin carbonyl carbons resonate prominently near **δ 160–165 ppm**. The aliphatic carbons in the methylene (-CH_2-) linkers are observed in the region of **δ 20–60 ppm**, with downfield shifts for carbons adjacent to electronegative atoms like oxygen or nitrogen. During the polymerization of a 7-amonomer, distinct and diagnostic changes are evident in both ^{1}H NMR and ^{13}C NMR spectra, which provide insights into the structural transformation from monomer to polymer. In the ^{1}H NMR spectrum, the singlet peak corresponding to the hydroxyl (-OH) proton, typically observed in the monomer, completely disappears. This disappearance indicates that the hydroxyl group has been consumed or chemically modified during the polymerization process, forming new covalent bonds. Furthermore, the peaks associated with protons near electronegative or functional groups in the monomer shift slightly downfield or up field in the polymer, reflecting the altered electronic and steric environment within the polymer backbone. In the ^{13}C NMR spectrum, the carbon signal attributed to the hydroxyl-bearing carbon in the monomer also vanishes, corroborating the chemical transformation of the hydroxyl group. Additionally, other carbon signals in the polymer exhibit slight shifts due to changes in hybridization, bond angles, and neighboring group effects introduced by the polymerization. These spectral shifts and peak changes are characteristic of polymer formation and serve as strong evidence of the structural modifications that occur during the conversion of the monomer to the polymer. So, based on NMR data confirm the successful polymerization and provide detailed information about the changes in the chemical environment of both protons and carbons in the resulting polymer.

This spectrum confirms the molecular complexity and functional group diversity, supporting the structural integrity of the triazole-linked aromatic polymer. The spectrum highlights the complexity and symmetry of the structure, confirming the incorporation of triazole linkages and nitro-functionalized coumarin derivatives in supplementary data.

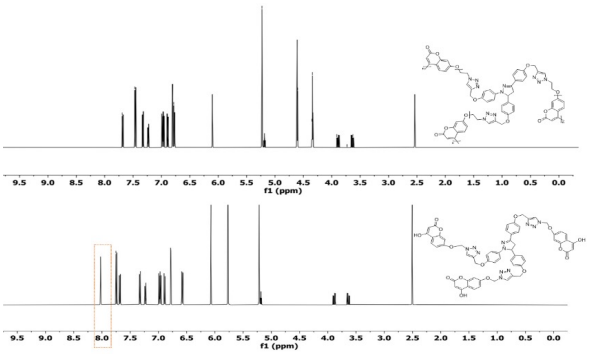

Figure 1: Comparison ^{1}H NMR spectrum of 7a monomer and 8a polymer

Antibacterial activity

All of the new synthesized derivatives (7a-e) were evaluated for their antibacterial properties against two gram positive and two gram negative. The antibacterial activities were investigated against *Staphylococcus aureus* (ATCC 23235), *Bacillus megaterium* (ATCC 14581), *Escherichia coli* (ATCC 8739) and *Proteus vulgaris* (PCM 2668). The results of the *in vitro* tests are summarized in Table 2 antibacterial activity of five synthesized compounds (8a, 8b, 8c, 8d, 8e) compared to Ampicillin, a standard antibiotic, against *Proteus vulgaris* PCM 2668. The x-axis denotes the concentration of the tested compounds (10 µM to 120 µM), including an untreated (UT) control, while the y-axis represents the percentage inhibition of bacterial growth **(Table 1) and Figure 2.** The untreated group displays negligible inhibition, confirming the specificity of the antibacterial effects to the compounds and Ampicillin. it, serving as the positive control, exhibits potent activity with over 95% bacterial inhibition at concentrations ≥70 µM, reinforcing its clinical relevance.

Among the synthesized compounds, 8b demonstrates the highest antibacterial activity, with significant inhibition even at lower concentrations and near-complete bacterial growth suppression at concentrations ≥70 µM, closely approximating the efficacy of Ampicillin. Compound 8a also displays dose-dependent antibacterial activity, though its inhibition levels remain consistently lower than 8b. Compound 8c shows moderate activity with inhibition increasing gradually until plateauing at higher concentrations, indicative of limited potency. By contrast, compounds 8d and 8e exhibit weak antibacterial activity, showing minimal inhibition even at the highest concentrations tested, highlighting their limited effectiveness against *Proteus vulgaris*.

Quantitative comparisons reveal that compound 8b achieves the highest activity fold (0.6) relative to Ampicillin, suggesting its strong antibacterial potential. Compounds 8a and 8c follow with activity folds of 0.43 and 0.33, respectively, reflecting moderate efficacy. In contrast, 8d and 8e exhibit the weakest activity (activity fold ~0.3), underscoring their significantly reduced effectiveness and the necessity for structural optimization to enhance their antimicrobial properties.

Moreover, against *Escherichia coli* ATCC 8739 highest inhibitions across all concentrations, exceeding 95% inhibition at concentrations of 70 µM. Among the synthesized compounds, 8b exhibits the highest antibacterial activity, reaching inhibition levels close to those of Ampicillin at concentrations above 70 µM. Compound 8a also shows a steady increase in inhibition with concentration, though it remains less effective than 8b. Compound 8c displays moderate activity, with inhibition levels plateauing at higher concentrations. In contrast, compounds 8d and 8e demonstrate significantly lower antibacterial activity, with only marginal improvements observed at higher concentrations, suggesting limited efficacy against *E. coli*. The UT group shows negligible inhibition, confirming that the observed activity is specific to the tested compounds. The antibacterial activity of five synthesized compounds (8a, 8b, 8c, 8d, 8e) was evaluated against *Staphylococcus aureus* ATCC 23235 and *Bacillus megaterium* ATCC 14581, results indicate that Ampicillin displayed the highest activity against both Gram-positive strains, achieving over 95% inhibition at concentrations of 70 µM and higher. Among the synthesized compounds, 8b showed the strongest antibacterial effects, reaching inhibition levels comparable to those of Ampicillin, particularly at concentrations above 70 µM. Compound 8a also demonstrated promising activity, with a steady increase in bacterial inhibition as concentration increased, although it remained slightly less effective than 8b. Compounds 8c and 8d exhibited moderate activity, with their inhibition plateauing at higher concentrations, indicating limited antibacterial potency. Compound 8e displayed the weakest activity, with negligible inhibition observed at lower concentrations and only slight improvements at higher concentrations.

In terms of activity fold compared to Ampicillin, compound 8b exhibited the highest fold value, approaching 0.8, indicating that its antibacterial potency is relatively close to Ampicillin, particularly at higher concentrations. Compound 8a demonstrated a moderate activity fold (around 0.5), suggesting moderate potential but still significantly less effective than Ampicillin. Compounds 8c and 8d had even lower activity folds (0.3 to 0.4), highlighting their limited antibacterial efficacy and the need for further

optimization. Compound 8e, with an activity fold closer to 0.2, demonstrated minimal antibacterial activity, underscoring its limited potential as a therapeutic agent without substantial structural modifications.

The **table 2** is the zone of inhibition (in mm) for various bacterial strains treated with 8a, 8b, 8c, 8d, and 8e, indicating the antibacterial efficacy of each treatment. For *E. coli* (ATCC 8739), treatment 8a produced the largest inhibition zone (25 ± 0.8 mm), reflecting strong antibacterial activity, while 8e showed the smallest zone (5 ± 1.2 mm), indicating weak activity. Against *P. vulgaris* (PCM 2668), 8b and 8d exhibited the largest inhibition zones (21 ± 1.2 mm and 21 ± 0.9 mm, respectively), whereas 8a showed moderate inhibition (15.3 ± 0.2 mm). For *S. aureus* (ATCC 23235), treatments 8b and 8d both had inhibition zones of 18 ± 0.8 mm, while 8a had the smallest zone (4 ± 0.8 mm), suggesting low activity. In the case of *B. megaterium* (ATCC 14581), 8a, 8c, and 8d produced similar zones of 13 ± 0.4 mm to 14 ± 0.5 mm, with 8e showing the smallest inhibition zone (6 ± 0.5 mm). Overall, treatment 8b demonstrated the most consistent and effective antibacterial activity, followed by 8d, while 8e exhibited the weakest zones of inhibition across all bacterial strains. These findings highlight the differential antibacterial potential of the treatments based on the size of the inhibition zones.

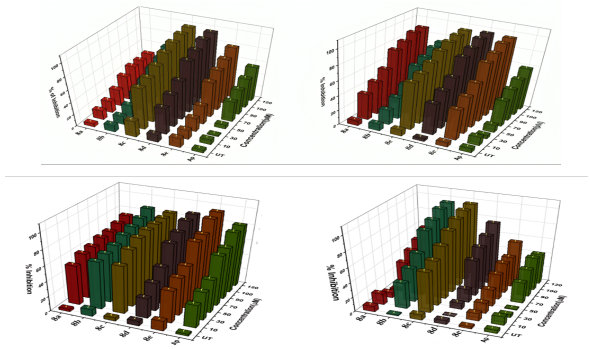

Figure 2: 3D bar graphs showing the concentration-dependent antibiofilm activity of the tested compound against various bacterial strains, as quantified by absorbance at 600 nm. (A) *E. coli (ATCC 8739)*, (B) *P. vulgaris (PCM 2668)*, (C) *S. aureus (ATCC 23235)*, and (D) *B. megaterium (ATCC 14581)*. Each set of bars corresponds to escalating concentrations of the compound (1.56 -100 µM) compared to the untreated control (UT). The observed reduction in optical density (OD) with higher concentrations highlights the compound's dose-dependent antibiofilm potential across different bacterial species, showcasing its efficacy in biofilm inhibition. *Values are represented as mean ± SD, n = 3.*

Molecular Docking Results

Molecular docking studies using the protein with PDB ID: 1KZN demonstrated a strong and stable binding interaction between the ligand 8a monomer and the protein's active site. The docking analysis revealed that the ligand formed several key interactions with critical residues in the binding pocket, contributing to its binding stability and specificity. Hydrogen bond interactions were observed with residues such as ASP45, ASN46, and LEU197, which play a crucial role in stabilizing the ligand within the binding site. Additionally, hydrophobic interactions with residues like ILE90 and π-stacking interactions with HIS116 and MET25 further enhanced the ligand's binding affinity (ΔG = -9.26 kcal/mol) **figure 3**.

Moreover, for the ampicillin and protein result analysis, the ligand forms conventional hydrogen bonds with residues **GLN135**, **THR163**, and **ASP73**, which are crucial for stabilizing the binding. Additionally, hydrophobic interactions with residues such as **ILE140** and **ARG142** contribute to the ligand's strong binding affinity. The presence of an unfavourable interaction (bump) with **ARG142** suggests potential areas for ligand optimization to improve binding efficacy (ΔG = -7.08 kcal/mol) **figure 4.** The 3D surface view of the docking results provided a clear visualization of the ligand fitting snugly within the protein's binding cavity, while the 3D interaction map highlighted the spatial arrangement of key residues involved in ligand binding. The 2D interaction schematic offered a detailed representation of the binding network, including conventional hydrogen bonds, carbon-hydrogen bonds, and hydrophobic contacts. These findings suggest that the ligand is well-suited to inhibit the activity of DNA gyrase, making it a promising candidate for further development as an antibacterial agent. The docking results provide valuable insights into the molecular basis of ligand-protein interactions, which can guide the rational design of more potent inhibitors to combat bacterial infections.

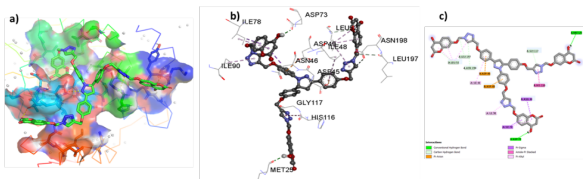

Figure 3: Molecular docking 8a monomer with PDB ID: 1KZN. (a) 3D surface view of the ligand within the protein binding site. (b) 3D interaction view highlighting key ligand-protein interactions. (c) 2D schematic of ligand-protein binding interactions (ΔG = -9.26 kcal/mol).

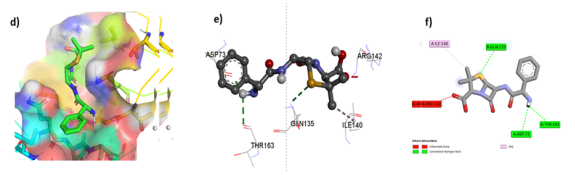

Figure 4: Molecular docking Ampicillin with PDB ID: 1KZN. (a) 3D surface view of the ligand within the protein binding site. (b) 3D interaction view highlighting key ligand-protein interactions. (c) 2D schematic of ligand-protein binding interactions (ΔG = -7.08 kcal/mol).

Table 1: Inhibitory concentration (IC_{50}) values of **8a-e** conjugates against gram-positive and gram-negative bacteria

Compound	E. *coli* (ATCC 8739)	P. *vulgaris* (PCM 2668)	S. *aureus* (ATCC 23235)	B. *megaterium* (ATCC 14581)
8a	49.30±59	28.95±2.8	50.23±1.6	76.46±0.8
8b	57±0.77	41.65±1.5	63.14±0.7	54.43±0.63
8c	35.68±1.2	32.48±0.9	71.84±1.2	55.19±1.8
8d	48.99±.6	54.43±1.4	45.97±1.2	76.46±1.2
8e	62.20±.8	64.89±0.5	81.76±1.6	81.35±2.3
Ampicillin	72.39±1.8	69.69±1.1	55.69±0.6	88.96±2.1

Table 2: Zone of Inhibition values of 8a-e conjugates against gram-positive and gram-negative bacteria

	Inhibition Zone Diameter (mm)				
Bacterial Strains	**8a**	**8b**	**8c**	**8d**	**8e**
E. coli (ATCC 8739)	25 ± 0.8	12 ± 0.9	15 ± 0.8	20 ± 0.9	5± 1.2
P. vulgaris (PCM 2668)	15.3 ± 0.2	21 ± 1.2	16 ± 0.2	21 ± 0.9	15± 0.9
S. aureus (ATCC 23235)	4 ± 0.8	18 ± 0.8	14 ± 0.8	18 ± 0.8	9.5± 0.6
B. megaterium (ATCC 14581)	13 ± 0.4	14 ± 0.5	13 ± 0.4	14 ± 0.5	6± 0.5

Materials and methods

All chemicals and solvents used in this study were obtained from certified international suppliers and used without further purification. Microbiological cultures and anaerobe indicator tests were procured from Sigma-Aldrich. Melting points of synthesized compounds were determined using a CIA 9300 electrochemical melting point apparatus by the open capillary method and were uncorrected. Reaction progress and compound purity were monitored by thin-layer chromatography (TLC) on precoated silica gel plates (GF254, Merck) using ethyl acetate–hexane (6:4) as the mobile phase.Infrared spectra were recorded using a Bruker Alpha ATR spectrometer, while UV–Visible spectra and kinetic studies were performed on a Varian UV–Visible spectrophotometer, with λmax values used for analysis. ^{1}H and ^{13}C NMR spectra were recorded on Bruker Avance 300 and 400 MHz instruments, with chemical shifts reported in ppm relative to tetramethylsilane as an internal standard. Spin–spin coupling patterns in ^{1}H NMR spectra were described as singlet, doublet, triplet, or multiplet. Antibacterial activity was evaluated against two Gram-positive and two Gram-negative bacterial strains: Staphylococcus aureus (ATCC 23235), Bacillus megaterium (ATCC 14581), Escherichia coli (ATCC 8739), and Proteus vulgaris (PCM 2668).

General Synthesis method

Synthesis of Compound 1

In a 100 mL round-bottom flask, **1.0 mmol** of the methoxy-substituted aromatic compound (e.g., methyl salicylate) and **1.0 mmol** of hydroxybenzaldehyde are dissolved in 10 mL of ethanol. To this, a catalytic amount of a base (e.g., 10 mol% sodium hydroxide or, **0.1 mmol**) is added dropwise under constant stirring. The reaction mixture is allowed to stir at room temperature for **6 hours**, during which the aldol condensation proceeds, yielding the chalcone derivative. After completion, the reaction mixture is neutralized using dilute acetic acid and poured into ice-cold water. The resulting precipitate is collected by filtration, washed with distilled water, and recrystallized from ethanol to obtain pure yield 90%.

Compound 1: (E)-1,3-bis(4-hydroxyphenyl)prop-2-en-1-one, Chemical Formula: $C_{15}H_{12}O_3$; ^{1}H NMR (500 MHz, DMSO-d_6) δ 9.35, 8.01, 8.01, 7.98, 7.98, 7.88, 7.88, 7.87, 7.86, 7.86, 7.86, 7.57, 7.54, 7.53, 7.53, 7.53, 7.53, 7.51, 7.51, 7.51, 7.51, 7.02, 7.01, 7.01, 7.00, 7.00, 6.99, 6.83, 6.82, 6.82, 6.81, 6.81, 6.80.

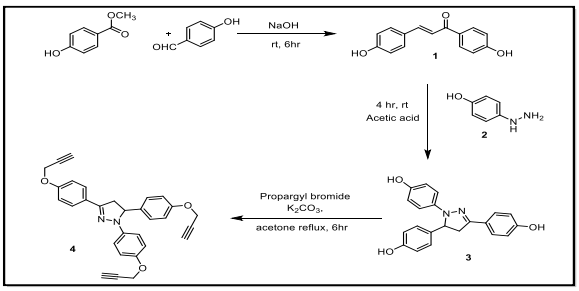

Scheme1: Synthesis of chalcone and its derivative propargyl bromide

Synthesis of Compound 3

1.2 mmol of Compound 1 and **1.2 mmol** of hydrazine derivative) are dissolved in a mixture of acetic acid (10 mL, **glacial acetic acid**). The reaction mixture is stirred at room temperature for **4 hours**. During this time, the condensation reaction occurs, forming the hydrazone-linked heterocyclic compound. The progress of the reaction is monitored by TLC (Thin Layer Chromatography) using an appropriate solvent system. Upon completion, the reaction mixture is diluted with water, and the product is extracted using ethyl acetate. The organic layer is dried over anhydrous sodium sulphate, and the solvent is removed under reduced pressure. The crude product is purified by column chromatography using a solvent system (hexane: ethyl acetate 4:6) to obtain pure 86 % yield.

Compound 3: 4,4',4''-(4,5-dihydro-1H-pyrazole-1,3,5-triyl)triphenol, Chemical Formula: $C_{21}H_{18}N_2O_3$; ^{1}H NMR (500 MHz, DMSO-d_6) δ 9.86,

9.26, 9.14, 7.67, 7.66, 7.66, 7.65, 7.64, 7.64, 7.35, 7.34, 7.34, 7.33, 7.33, 7.32, 7.21, 7.20, 7.20, 7.20, 7.19, 7.19, 7.18, 7.18, 6.87, 6.87, 6.86, 6.86, 6.85, 6.85, 6.85, 6.84, 6.84, 6.84, 6.83, 6.63, 6.62, 6.62, 6.61, 6.60, 6.60, 5.20, 5.20, 5.19, 5.18, 5.17, 5.17, 3.91, 3.90, 3.88, 3.87, 3.66, 3.65, 3.63, 3.62.

Synthesis of Compound 4

To synthesize Compound 4, 1.0 mmol of the hydroxy-substituted hydrazone derivative is dissolved in 10 mL of dry acetone, and 2.0 mmol of propargyl bromide with 2.0 mmol of K_2CO_3 is added. The mixture is refluxed for 6 hours. After cooling, the mixture is filtered to remove salts, and the filtrate is concentrated and extracted with ethyl acetate. The organic layer is washed, dried, and concentrated. The crude product is purified by column chromatography (hexane: ethyl acetate 5:5) to obtain pure 89 % yield.

Synthesis of Compound 5a-e

In a 50 mL round-bottom flask, 1.0 mmol of the hydroxy-substituted aromatic compound is dissolved in 10 mL of dry acetone. To this, 1.2 mmol of dibromo alkane and 2.0 mmol of potassium carbonate (K_2CO_3) are added. The reaction mixture is refluxed under stirring for 6 hours. After completion, the reaction mixture is filtered to remove inorganic salts, and the solvent is evaporated under reduced pressure. The crude product is purified by column chromatography (hexane: methanol 4:6) 82% yield obtained.

Compound 5a: 7-(bromomethoxy)-4-hydroxy-2H-chromen-2-one, Chemical Formula: $C_{10}H_7BrO_4$; ^{1}H NMR (500 MHz, DMSO-d_6) δ 7.76, 7.74, 6.84, 6.84, 6.69, 6.69, 6.68, 6.67, 6.07, 5.55. ^{13}C NMR (125 MHz, Common NMR Solvents) δ 166.65, 162.98, 161.98, 155.43, 127.01, 111.21, 103.97, 101.36, 88.40, 60.75.

Compound 5b: 7-(bromoethoxy)-4-hydroxy-2H-chromen-2-one, Chemical Formula: $C_{10}H_9BrO_4$; ^{1}H NMR (500 MHz, DMSO-d_6) δ 7.76, 7.74, 6.81, 6.80, 6.61, 6.61, 6.60, 6.59, 6.07, 4.36, 4.35, 4.34, 3.76, 3.76, 3.75. ^{13}C NMR (125 MHz, Common NMR Solvents) δ 166.65, 162.98, 161.98, 155.43, 127.01, 111.21, 103.97, 101.36, 88.40, 60.75.

Compound 5c: 7-(3-bromopropoxy)-4-hydroxy-2H-chromen-2-one, Chemical Formula: $C_{12}H_{11}BrO_4$; ^{1}H NMR (500 MHz, DMSO-d6) δ 7.76, 7.74, 6.81, 6.80, 6.61, 6.61, 6.60, 6.59, 6.07, 4.11, 4.10, 4.09, 3.61, 3.60, 3.59, 2.48, 2.47, 2.46, 2.45, 2.44. ^{13}C NMR (125 MHz, Common NMR Solvents) δ 166.65, 162.97, 162.64, 155.44, 126.99, 111.27, 103.97, 101.67, 88.38, 67.22, 32.34, 29.97.

Compound 5d: 7-(4-bromobutoxy)-4-hydroxy-2H-chromen-2-one, Chemical Formula: $C_{13}H_{13}BrO_4$; ^{1}H NMR (500 MHz, DMSO-d_6) δ 7.76, 7.74, 6.81, 6.80, 6.61, 6.61, 6.60, 6.59, 6.07, 4.10, 4.08, 4.07, 3.50, 3.49, 3.48, 1.94, 1.93, 1.93, 1.93, 1.92, 1.92, 1.92, 1.92, 1.91, 1.91, 1.91, 1.91, 1.90, 1.90, 1.90, 1.90, 1.89, 1.89, 1.86, 1.86, 1.85, 1.85, 1.84, 1.84, 1.84, 1.83, 1.83, 1.83, 1.83, 1.82, 1.82, 1.82, 1.81, 1.81, 1.80. ^{13}C NMR (125 MHz, Common NMR Solvents) δ 166.65, 162.97, 162.62, 155.44, 126.99, 111.27, 103.97, 101.61, 88.38, 68.04, 33.43, 29.83, 28.43.

Compound 5e: 7-((5-bromopentyl)oxy)-4-hydroxy-2H-chromen-2-one, Chemical Formula: $C_{14}H_{15}BrO_4$; ^{1}H NMR (500 MHz, DMSO-d_6) δ 7.76, 7.74, 6.81, 6.80, 6.61, 6.61, 6.60, 6.59, 6.07, 4.06, 4.05, 4.03, 3.44, 3.43, 3.42, 1.82, 1.81, 1.81, 1.81, 1.80, 1.80, 1.80, 1.80, 1.79, 1.79, 1.78, 1.77, 1.74, 1.73, 1.72, 1.72, 1.72, 1.71, 1.71, 1.71, 1.70, 1.70, 1.69, 1.69, 1.68, 1.68, 1.64, 1.64, 1.63, 1.62, 1.61, 1.61, 1.60, 1.60, 1.59, 1.58, 1.58. ^{13}C NMR (125 MHz, Common NMR Solvents) δ 166.65, 162.97, 162.62, 155.44, 126.99, 111.27, 103.97, 101.61, 88.38, 68.83, 33.27, 30.38, 27.03, 26.81.

Synthesis of Compound 6a-e

In a separate reaction, 1.0 mmol of Compound 5 is dissolved in 10 mL of ethanol, and 1.2 mmol of sodium azide (NaN_3) is added. The mixture is refluxed for 6 hours, allowing the substitution reaction to occur, replacing the bromine atom with an azide group. The progress of the reaction is monitored by TLC. After completion, the reaction mixture is cooled, and the solvent is removed under reduced pressure. The residue is purified by recrystallization or column chromatography (hexane: methanol 6:4) 72% yield obtained.

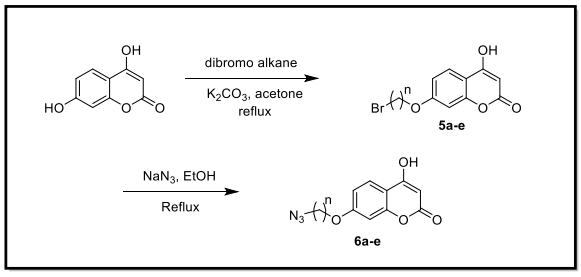

Scheme 2: synthesis of Coumarin bromide and coumarin azide

Synthesis of monomer 7a-e

compound 4 (1.0 mmol) and compound 6 (1.0 mmol) were dissolved in 10 mL of dry N,N-dimethylformamide (DMF) in a dry round-bottom flask under an inert nitrogen atmosphere. Potassium carbonate (K_2CO_3, 2.0 mmol) was added to the reaction mixture as a base, followed by copper(I) iodide (CuI, 1mmol%) as a catalyst. The reaction mixture was stirred and heated to 120°C under reflux for 10 hours. The progress of the reaction was monitored using thin-layer chromatography (TLC). After completion, the reaction mixture was cooled to room temperature and

diluted with 50 mL of water to precipitate the crude product. The precipitate was extracted with ethyl acetate (3 × 20 mL), and the combined organic layers were washed with water and brine, followed by drying over anhydrous sodium sulphate. The solvent was removed under reduced pressure to yield the crude product purified with the (methanol: hexane 4:6) obtained yield 95%.

Compound 7a: 7,7',7''-(((((((4,5-dihydro-1H-pyrazole-1,3,5-triyl)tris(benzene-4,1-diyl))tris(oxy))tris(methylene))tris(1H-1,2,3-triazole-4,1-diyl))tris(methylene))tris(oxy))tris(4-hydroxy-2H-chromen-2-one), Chemical Formula: $C_{60}H_{45}N_{11}O_{15}$; ^{1}H NMR (500 MHz, DMSO-d6) δ 8.03, 8.02, 8.02, 7.75, 7.74, 7.70, 7.69, 7.69, 7.68, 7.68, 7.67, 7.34, 7.34, 7.33, 7.32, 7.32, 7.32, 7.24, 7.24, 7.24, 7.23, 7.23, 7.22, 7.22, 7.00, 6.99, 6.99, 6.98, 6.98, 6.97, 6.97, 6.97, 6.96, 6.95, 6.95, 6.90, 6.90, 6.90, 6.89, 6.88, 6.88, 6.78, 6.78, 6.59, 6.58, 6.57, 6.57, 6.07, 5.77, 5.77, 5.22, 5.22, 5.21, 5.20, 5.19, 5.18, 5.17, 5.17, 3.91, 3.90, 3.88, 3.87, 3.66, 3.65, 3.63, 3.62. ^{13}C NMR (125 MHz, Common NMR Solvents) δ 166.84, 166.75, 166.65, 163.11, 163.05, 162.98, 161.12, 161.11, 161.00, 159.63, 157.17, 155.44, 155.42, 155.40, 153.13, 148.99, 144.43, 144.39, 144.35, 139.01, 133.39, 128.75, 127.68, 126.97, 126.95, 126.94, 126.48, 121.45, 121.41, 121.38, 118.65, 116.70, 115.42, 115.21, 112.38, 112.37, 112.36, 104.15, 104.06, 103.97, 102.67, 102.63, 102.60, 88.59, 88.49, 88.40, 74.19, 74.16, 74.12, 65.58, 57.90, 57.87, 57.84, 40.71.

Compound 7b: 7,7',7''-(((((((4,5-dihydro-1H-pyrazole-1,3,5-triyl)tris(benzene-4,1-diyl))tris(oxy))tris(methylene))tris(^{1}H-1,2,3-triazole-4,1-diyl))tris(ethane-2,1-diyl))tris(oxy))tris(4-hydroxy-2H-chromen-2-one); Chemical Formula: $C_{63}H_{51}N_{11}O_{15}$; ^{1}H NMR (500 MHz, DMSO-d6) δ 8.08, 8.08, 8.07, 8.07, 7.76, 7.74, 7.70, 7.69, 7.69, 7.68, 7.68, 7.67, 7.34, 7.34, 7.33, 7.32, 7.32, 7.32, 7.24, 7.24, 7.24, 7.23, 7.23, 7.22, 7.22, 7.00, 6.99, 6.99, 6.98, 6.98, 6.97, 6.97, 6.97, 6.96, 6.95, 6.95, 6.90, 6.90, 6.90, 6.89, 6.88, 6.88, 6.82, 6.82, 6.61, 6.61, 6.60, 6.59, 6.07, 5.23, 5.23, 5.20, 5.19, 5.18, 5.17, 5.17, 4.62, 4.61, 4.60, 4.35, 4.35, 4.35, 4.34, 4.34, 4.34, 4.33, 4.33, 4.33, 3.91, 3.90, 3.88, 3.87, 3.66, 3.65, 3.63, 3.62. ^{13}C NMR (125 MHz, Common NMR Solvents) δ 166.84, 166.75, 166.65, 163.10, 163.03, 162.97, 162.62, 162.60, 162.57, 159.63, 157.17, 155.49, 155.47, 155.45, 153.13, 148.98, 143.02, 142.98, 142.94, 139.01, 133.39, 128.75, 127.68, 127.02, 127.00, 126.99, 126.48, 121.51, 121.46, 121.41, 118.65, 116.70, 115.42, 115.21, 111.37, 111.36, 111.35, 104.15, 104.06, 103.97, 101.81, 101.77, 101.74, 88.57, 88.47, 88.38, 66.30, 66.27, 66.24, 65.58, 57.90, 57.87, 57.84, 49.24, 49.19, 49.14, 40.71.

Compound 7c: 7,7',7''-(((((((4,5-dihydro-1H-pyrazole-1,3,5-triyl)tris(benzene-4,1-diyl))tris(oxy))tris(methylene))tris(^{1}H-1,2,3-triazole-4,1-diyl))tris(propane-3,1-diyl))tris(oxy))tris(4-hydroxy-2H-chromen-2-one); Chemical Formula: $C_{66}H_{57}N_{11}O_{15}$; ^{1}H NMR (500 MHz, DMSO-*d*6) δ 8.27, 8.27, 8.26, 8.26, 7.76, 7.74, 7.70, 7.69, 7.69, 7.68, 7.68, 7.67, 7.34, 7.34, 7.33, 7.32, 7.32, 7.32, 7.24, 7.24, 7.24, 7.23, 7.23, 7.22, 7.00, 6.99, 6.99, 6.98, 6.98, 6.97, 6.97, 6.97, 6.96, 6.95, 6.95, 6.90, 6.90, 6.90, 6.89, 6.88, 6.88, 6.81, 6.80, 6.61, 6.61, 6.60, 6.59, 6.07, 5.23, 5.23, 5.20, 5.19, 5.18, 5.17, 4.21, 4.20, 4.19, 4.18, 4.18, 4.17, 4.17, 4.16, 4.16, 3.91, 3.90, 3.88, 3.87, 3.66, 3.65, 3.63, 3.62, 2.28, 2.26, 2.25, 2.24, 2.22. ^{13}C NMR (125 MHz, Common NMR Solvents) δ 166.84, 166.75, 166.65, 163.10, 163.03, 162.97, 162.62, 162.60, 162.57, 159.63, 157.17, 155.49, 155.47, 155.45, 153.13, 148.98, 143.02, 142.98, 142.94, 139.01, 133.39, 128.75, 127.68, 127.02, 127.00, 126.99, 126.48, 121.51, 121.46, 121.41, 118.65, 116.70, 115.42, 115.21, 111.37, 111.36, 111.35, 104.15, 104.06, 103.97, 101.81, 101.77, 101.74, 88.57, 88.47, 88.38, 66.30, 66.27, 66.24, 65.58, 57.90, 57.87, 57.84, 49.24, 49.19, 49.14, 40.71.

Compound 7d: 7,7',7''-(((((((4,5-dihydro-1H-pyrazole-1,3,5-triyl)tris(benzene-4,1-diyl))tris(oxy))tris(methylene))tris(1H-1,2,3-triazole-4,1-diyl))tris(butane-4,1-diyl))tris(oxy))tris(4-hydroxy-2H-chromen-2-one); Chemical Formula: $C_{69}H_{63}N_{11}O_{15}$;

^{1}H NMR (500 MHz, DMSO-*d*$_6$) δ 8.27, 8.27, 8.26, 8.26, 7.76, 7.74, 7.70, 7.69, 7.69, 7.68, 7.68, 7.67, 7.34, 7.34, 7.33, 7.32, 7.32, 7.32, 7.24, 7.24, 7.24, 7.23, 7.23, 7.22, 7.22, 7.00, 6.99, 6.99, 6.98, 6.98, 6.97, 6.97, 6.97, 6.96, 6.95, 6.95, 6.90, 6.90, 6.90, 6.89, 6.88, 6.88, 6.81, 6.80, 6.61, 6.61, 6.60, 6.59, 6.07, 5.23, 5.23, 5.20, 5.19, 5.18, 5.17, 5.17, 4.28, 4.28, 4.27, 4.26, 4.25, 4.25, 4.02, 4.01, 4.00, 3.91, 3.90, 3.88, 3.87, 3.66, 3.65, 3.63, 3.62, 1.95, 1.95, 1.94, 1.94, 1.94, 1.93, 1.93, 1.92, 1.92, 1.91, 1.91, 1.91, 1.90, 1.90, 1.82, 1.81, 1.80, 1.80, 1.80, 1.80, 1.79, 1.79, 1.79, 1.79, 1.78, 1.78, 1.78, 1.78, 1.77, 1.77, 1.76, 1.76. ^{13}C NMR (125 MHz, Common NMR Solvents) δ 166.84, 166.75, 166.65, 163.10, 163.03, 162.97, 162.74, 162.68, 162.63, 159.63, 157.17, 155.49, 155.47, 155.44, 153.13, 148.98, 142.44, 142.40, 142.35, 139.01, 133.39, 128.75, 127.68, 127.02, 127.01, 126.99, 126.48, 122.22, 122.14, 122.06, 118.65, 116.70, 115.42, 115.21, 111.29, 111.28, 111.27, 104.15, 104.06, 103.97, 101.67, 101.64, 101.61, 88.57, 88.47, 88.38, 67.92, 67.90, 67.87, 65.58,

57.90, 57.87, 57.84, 50.60, 50.55, 50.51, 40.71, 26.77, 26.74, 26.72, 26.35, 26.32, 26.30.

Compound 7e: 7,7',7''-(((((((4,5-dihydro-1H-pyrazole-1,3,5-triyl)tris(benzene-4,1-diyl))tris(oxy))tris(methylene))tris(1H-1,2,3-triazole-4,1-diyl))tris(pentane-5,1-diyl))tris(oxy))tris(4-hydroxy-2H-chromen-2-one);

Chemical Formula: $C_{72}H_{69}N_{11}O_{15}$;

^{1}H NMR (500 MHz, DMSO-d_6) δ 8.27, 8.27, 8.26, 8.26, 7.76, 7.74, 7.70, 7.69, 7.69, 7.68, 7.68, 7.67, 7.34, 7.34, 7.33, 7.32, 7.32, 7.32, 7.24, 7.24, 7.24, 7.23, 7.23, 7.22, 7.00, 6.99, 6.99, 6.98, 6.98, 6.97, 6.97, 6.97, 6.96, 6.95, 6.95, 6.90, 6.90, 6.90, 6.89, 6.88, 6.88, 6.81, 6.80, 6.61, 6.61, 6.60, 6.59, 6.07, 5.23, 5.23, 5.20, 5.19, 5.18, 5.17, 4.23, 4.23, 4.22, 4.22, 4.20, 4.20, 4.00, 3.99, 3.98, 3.91, 3.90, 3.88, 3.87, 3.66, 3.65, 3.63, 3.62, 1.91, 1.89, 1.88, 1.87, 1.85, 1.70, 1.69, 1.68, 1.67, 1.66, 1.65, 1.53, 1.53, 1.52, 1.50, 1.49, 1.48, 1.48. ^{13}C NMR (125 MHz, Common NMR Solvents) δ 166.84, 166.75, 166.65, 163.10, 163.03, 162.97, 162.74, 162.68, 162.63, 159.63, 157.17, 155.49, 155.47, 155.44, 153.13, 148.98, 142.44, 142.40, 142.35, 139.01, 133.39, 128.75, 127.68, 127.02, 127.01, 126.99, 126.48, 122.22, 122.14, 122.06, 118.65, 116.70, 115.42, 115.21, 111.29, 111.28, 111.27, 104.15, 104.06, 103.97, 101.67, 101.64, 101.61, 88.57, 88.47, 88.38, 67.92, 67.90, 67.87, 65.58, 57.90, 57.87, 57.84, 50.60, 50.55, 50.51, 40.71, 26.77, 26.74, 26.72, 26.35, 26.32, 26.30.

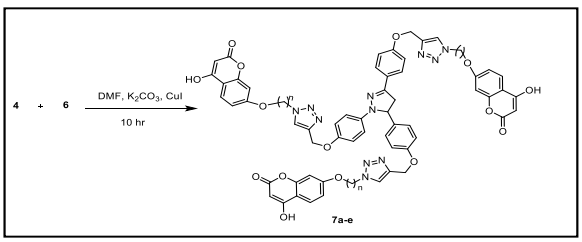

Scheme 3: Synthesis of monomer using CuI and K_2CO_3

Table 1: Optimization reaction with different catalyst mol ration

Entry	CuI (mol %ratio)	Solvent	Temperature (°C)	Time (hours)	Base	Yield (%)
1	0.05	DMSO	80	18	K_2CO_3	70
2	0.1	DMF	100	8	NaOH	69
3	0.2	Toluene	120	10	Cs_2CO_3	65
4	0.3	Ethanol	60	4	Et_3N	65
5	0.3	Ethanol	60	8	Et_3N	69
6	0.5	Acetonitrile	90	16	K_2CO_3	85
7	1	THF	70	5	Pyridine	80
8	0.5	DMF	100	8	KOH	73
9	1	DMF	100	12	KOH	92
10	1	DMF	100	10	K_2CO_3	95

Polymerization of Compound 8

Compound 7 was polymerized using a copper(I)-catalyzed azide-alkyne cycloaddition (CuAAC) reaction, leveraging its functional azide and alkyne groups for chain-growth polymerization. To begin, compound 7 (1.0 mmol) was dissolved in dry N,N-dimethylformamide (DMF, 10 mL) under a nitrogen atmosphere to prevent oxidation. A di-functional alkyne (1.0 mmol), was added as a crosslinking agent to promote polymerization. Potassium carbonate (K_2CO_3, 0.2 mmol) was added as a base, along with copper(I) iodide (CuI, 1 mmol %) as the catalyst to initiate the click polymerization reaction.

The reaction mixture was stirred and heated to 120°C under reflux for 12–24 hours. The mixture was cooled to room temperature and poured into a non-solvent, such as cold methanol, to precipitate the polymer. The precipitate was collected by filtration, washed thoroughly with methanol to remove any unreacted monomer or catalyst residues, and dried under vacuum at 60°C for 12 hours.

Compound 8a polymer: ^{1}H NMR (500 MHz, DMSO-d_6) δ 7.69, 7.47, 7.32, 7.25, 7.22, 6.98, 6.90, 6.89, 6.88, 6.79, 6.76, 5.23, 5.18, 5.17, 4.60, 4.35, 4.34, 3.91, 3.73, 3.63. ^{13}C NMR (125 MHz, Common NMR Solvents) δ 166.65, 163.11, 163.05, 162.98, , 161.11, 161.00, 159.63, 157.17, 155.44, 155.42, 155.40, 153.13, 148.99, 144.43, 144.39, 144.35, , 133.39, 128.75, 127.68, 126.97, 126.95, 126.94, 126.48, 121.45, 121.41, 121.38, 118.65, 116.70, 115.42, 112.38, 112.37, 112.36, 104.06, 103.97, 102.67, 102.63, , 88.59, 88.49, 88.40, 74.19, 74.16, 74.12, 65.58, 57.90, 57.87, 57.84,

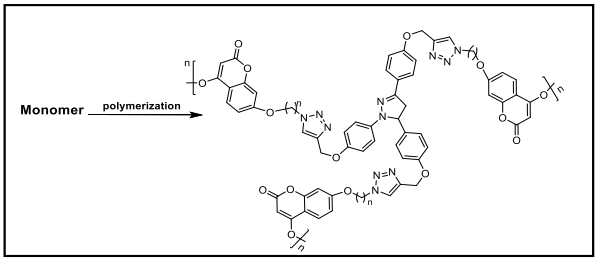

Scheme 4: polymerization of heterocyclic monomer

Antimicrobial activity

The nutrient broth was prepared and autoclaved for 20 minutes at 120 psi. two sets of gram-negative and gram-positive bacteria were inoculated and incubated at 37 °C for 24 hours. Then, each well was inoculated with a microbial inoculum prepared in the same medium after dilution of standardized microbial suspension adjusted to 0.5 McFarland scale (10^8 CFU/mL). 180 µl of the cell suspension was seeded in each of the 96 well plates and 20 µl of different concentrations of the test compounds and the standard was added. The wells without test compound were considered as control and streptomycin was used as standard. After mixing, the 96-well plates were incubated at 37 °C for 24 hours. After incubation, the absorbance of each well was recorded at 600 nm using Read well Touch Automatic Elisa Plate Reader (Robonik India Private Limited). All the experiments

were performed in triplicates and the growth percentage was calculated using the formula:

Percentage growth inhibition= Ti/C x 100

where Ti = Growth of the microorganisms in the presence of a drug, and C = Control growth

Zone of inhibition assays

The *Kirby-Bauer Disk Susceptibility Test* is a standardized method used to determine the sensitivity of bacteria to antibiotics. The process begins by preparing a bacterial suspension using 3-5 well-isolated colonies from a pure culture, which are suspended in sterile saline or broth and adjusted to match the 0.5 McFarland turbidity standard. A sterile cotton swab is then dipped into the bacterial suspension, excess liquid is removed, and the swab is used to streak the entire surface of a Mueller-Hinton agar plate to ensure even distribution. The plate is allowed to dry for approximately 5 minutes at room temperature. Antibiotic-impregnated disks are then placed onto the agar surface using sterile forceps, ensuring they are evenly spaced and pressed gently for full contact. The plates are inverted and incubated at 35°C ± 2°C for 18-24 hours. After incubation, the zones of inhibition (clear areas around the disks) are measured in millimetres using a ruler or callipers.

Molecular Docking:

Ligand preparation

Molecular docking involves simulating the interaction between a ligand and a target protein to predict binding affinity and orientation, which ensures the ligand is in its optimal form for docking. This involves retrieving the ligand structure from databases like PubChem or creating it using molecular modelling software. The ligand is then optimized by removing any steric clashes, adding hydrogens, and assigning appropriate charges using tools like Open Babel or AutoDockTools. Additionally, its energy is minimized to achieve a stable conformation.

Choose Protein

Selecting the appropriate protein is a critical step in molecular docking as it directly influences the accuracy and reliability of the docking results. In this study, the protein with PDB ID: **1KZN**, which represents DNA gyrase, was selected from the Protein Data Bank (PDB). DNA gyrase is a type II topoisomerase that plays an essential role in bacterial cells by introducing negative supercoils into DNA. This process is vital for relieving torsional strain during key cellular processes such as DNA replication, transcription, and recombination. By maintaining the structural and functional integrity of the bacterial genome, DNA gyrase ensures the proper functioning of bacterial cells.

The significance of targeting DNA gyrase lies in its absence in humans, making it an ideal target for the development of selective antibacterial agents with minimal off-target effects. Inhibiting DNA gyrase disrupts bacterial DNA processes, ultimately leading to cell death. This mechanism of action underpins the effectiveness of many widely used antibiotics, such as fluoroquinolones. Given the growing threat of antibiotic resistance, studying DNA gyrase through molecular docking is crucial for designing novel inhibitors that can combat resistant bacterial strains.

To maximize the precision of docking studies, the selected protein must meet specific criteria. High-resolution structural data (preferably below 2.5 Å) is essential to ensure the accuracy of atomic-level interactions. Additionally, the protein should be in its active or functional conformation with a clearly defined binding site. The presence of co-crystallized ligands in the protein structure is particularly advantageous, as it helps identify and validate the active site for docking. These factors enable the molecular docking process to accurately simulate biological interactions and provide reliable insights into ligand binding and protein-ligand interactions.

Protein preparation

The second step is protein preparation for the target protein, identified by its PDB ID: 1KZN. The structure is downloaded from the Protein Data Bank and processed to remove water molecules, heteroatoms, and co-crystallized ligands that may interfere with docking. Hydrogen atoms are added to account for protonation states, and any missing residues or side chains are rebuilt using tools Auto dock software. The protein structure is then energy-minimized, and a grid box is defined around the active site to guide the docking process. These preparatory steps ensure accurate and reliable docking results.

Conclusion

This study presents the successful synthesis, characterization, and evaluation of chalcone- and coumarin-based heterocyclic polymers, highlighting their potential as novel antibacterial agents. These polymers demonstrated broad-spectrum antibacterial activity against both Gram-positive and Gram-negative bacterial strains, including *Staphylococcus aureus* (ATCC 23235), *Bacillus megaterium* (ATCC 14581), *Escherichia coli* (ATCC 8739), and *Proteus vulgaris* (PCM 2668). Compound 8b emerged as the most effective, achieving inhibition levels of 57.0% against *E. coli* and 63.1% against *S. aureus*, while compound 8e exhibited outstanding activity, with 81.7% and 81.3% inhibition against *S. aureus* and *B. megaterium*, respectively. The antibacterial efficacy of these

polymers was attributed to their ability to disrupt bacterial membranes, inhibit key enzymes, and induce oxidative stress. Additionally, their structural flexibility, enhanced stability, and low cytotoxicity contribute to their potential as safe and effective therapeutic agents. Comparative analyses revealed that compounds such as 8b demonstrated activity comparable to Ampicillin, a widely used standard antibiotic, further validating their potential clinical relevance. These findings underscore the significance of chalcone- and coumarin-based heterocyclic polymers in addressing the urgent global challenge of antimicrobial resistance. Their multifunctional properties, biocompatibility, and structural tunability make them promising candidates for further development as next-generation antibacterial materials. Future research should focus on optimizing their design for enhanced selectivity and efficacy, exploring their mechanisms of action in greater detail, and conducting in vivo studies to evaluate their therapeutic potential.This work provides a strong foundation for advancing heterocyclic polymers as a valuable addition to the arsenal of antimicrobial agents, offering hope in the fight against multidrug-resistant bacterial infections.

References:

[1] Zipperer, A., *et al.*, 2016, "Human Commensals Producing a Novel Antibiotic Impair Pathogen Colonization," *Nature*, 535(7613), pp. 511–516.

[2] Tsai, C. J.-Y., Loh, J. M. S., and Proft, T., 2016, "Galleria mellonella Infection Models for the Study of Bacterial Diseases and for Antimicrobial Drug Testing," *Virulence*, 7(3), pp. 214–229.

[3] Tian, Z., Xu, J., Liu, B., Tan, Q., and Xu, B., 2018, "Copper-Catalyzed Synthesis of Polysubstituted Pyrroles through [3+1+1] Cycloaddition Reaction of Nitrones and Isocyanides," *Org. Lett.*, 20(9), pp. 2603–2606.

[4] Tahri, A., Buysens, K. J., Van Der Eycken, E. V., Vandenberghe, D. M., and Hoornaert, G. J., 1998, "Synthesis of α-Carbolines and β-Carbolinones via Intramolecular Diels–Alder Reactions of 2(1H)-Pyrazinones," *Tetrahedron*, 54(43), pp. 13211–13226.

[5] Soto-Rodriguez, S. A., Cabanillas-Ramos, J., Alcaraz, U., Gomez-Gil, B., and Romalde, J. L., 2013, "Identification and Virulence of *Aeromonas dhakensis*, *Pseudomonas mosselii* and *Microbacterium paraoxydans* Isolated from Nile Tilapia, *Oreochromis niloticus*, Cultivated in Mexico," *J. Appl. Microbiol.*, 115(3), pp. 654–662.

[6] Sharma, P., Makkar, R., and Singh, S., 2016, "Antibacterial, Antifungal and Antioxidant Activities of Substituted 4H-1,4-Benzothiazines," *Int. J. Pharm. Sci. Rev. Res.*, 8, pp. 156–159.

[7] Shadmon, H., Basu, A., Eckhard, L. H., Domb, A. J., and Beyth, N., 2018, "Synthesis, Characterization and Antibacterial Activity of Heterocyclic Quaternary Ammonium Polymers," *New J. Chem.*, 42(18), pp. 15427–15435.

[8] Peters, B. M., Jabra-Rizk, M. A., O'May, G. A., Costerton, J. W., and Shirtliff, M. E., 2012, "Polymicrobial Interactions: Impact on Pathogenesis and Human Disease," *Clin. Microbiol. Rev.*, 25(1), pp. 193–213.

[9] Otto, M., 2010, "Basis of Virulence in Community-Associated Methicillin-Resistant *Staphylococcus aureus*," *Annu. Rev. Microbiol.*, 64(1), pp. 143–162.

[10] Muteeb, G., Rehman, M. T., Shahwan, M., and Aatif, M., 2023, "Origin of Antibiotics and Antibiotic Resistance, and Their Impacts on Drug Development: A Narrative Review," *Pharmaceuticals*, 16(11), p. 1615.

[11] Moroi, K., and Sato, T., 1975, "Comparison Between Procaine and Isocarboxazid Metabolism *In Vitro* by a Liver Microsomal Amidase-Esterase," *Biochem. Pharmacol.*, 24(16), pp. 1517–1521.

[12] Mohamad, N. R., Marzuki, N. H. C., Buang, N. A., Huyop, F., and Wahab, R. A., 2015, "An Overview of Technologies for Immobilization of Enzymes and Surface Analysis Techniques for Immobilized Enzymes," *Biotechnol. Biotechnol. Equip.*, 29(2), pp. 205–220.

[13] McAuliffe, O., Ross, R. P., and Hill, C., 2001, "Lantibiotics: Structure, Biosynthesis and Mode of Action," *FEMS Microbiol. Rev.*, 25(3), pp. 285–308.

[14] Lu, S., Ding, C.-H., and Xu, B., 2023, "Triple-Consecutive Isocyanide Insertions with Aldehydes: Synthesis of 4-Cyanooxazoles," *Org. Lett.*, 25(5), pp. 849–854.

[15] Leonard, B. E., 1975, "Neurochemical and Neuropharmacological Aspects of Depression," *Int. Rev. Neurobiol.*, 18, pp. 357–387.

[16] Kuroda, M., *et al.*, 2001, "Whole Genome Sequencing of Meticillin-Resistant *Staphylococcus aureus*," *Lancet*, 357(9264), pp. 1225–1240.

[17] Kluytmans, J. A. J. W., and Wertheim, H. F. L., 2005, "Nasal Carriage of *Staphylococcus aureus*

and Prevention of Nosocomial Infections," *Infection*, 33(1), pp. 3–8.

[18] Khan, M. H., *et al.*, 2017, "Few-Atomic-Layered Hexagonal Boron Nitride: CVD Growth, Characterization, and Applications," *Mater. Today*, 20(10), pp. 611–628.

[19] Jarraud, S., *et al.*, 2002, "Relationships Between *Staphylococcus aureus* Genetic Background, Virulence Factors, agr Groups (Alleles), and Human Disease," *Infect. Immun.*, 70(2), pp. 631–641.

[20] Iwase, T., *et al.*, 2010, "*Staphylococcus epidermidis* Esp Inhibits *Staphylococcus aureus* Biofilm Formation and Nasal Colonization," *Nature*, 465(7296), pp. 346–349.

[21] Hendrickson, W. A., and Ward, K. B., 1975, "Atomic Models for the Polypeptide Backbones of Myohemerythrin and Hemerythrin," *Biochem. Biophys. Res. Commun.*, 66(4), pp. 1349–1356.

[22] Hardy, B. L., *et al.*, 2019, "*Corynebacterium pseudodiphtheriticum* Exploits *Staphylococcus aureus* Virulence Components in a Novel Polymicrobial Defense Strategy," *mBio*, 10(1), pp. e02491–18.

[23] Götz, F., Perconti, S., Popella, P., Werner, R., and Schlag, M., 2014, "Epidermin and Gallidermin: Staphylococcal Lantibiotics," *Int. J. Med. Microbiol.*, 304(1), pp. 63–71.

[24] Giangrande, M., Kim, Y. W., and Mizukami, H., 1975, "N-Terminal Spin Label Studies of Hemoglobin: Ligand and pH Dependence," *Biochim. Biophys. Acta*, 412(1), pp. 187–193.

[25] Filkins, L. M., *et al.*, 2015, "Coculture of *Staphylococcus aureus* with *Pseudomonas aeruginosa* Drives *S. aureus* Towards Fermentative Metabolism and Reduced Viability in a Cystic Fibrosis Model," *J. Bacteriol.*, 197(14), pp. 2252–2264.

[26] El-Essawy, F. A., and Odah, M. A. A., 2024, "Design and Synthesis of Polyheterocyclic Compounds Containing Pyrazolopyridopyrimidine Nucleus with Antimicrobial Activities," *ChemistryOpen*, 13(6).

[27] Desplat, V., *et al.*, 2016, "Synthesis and Evaluation of the Cytotoxic Activity of Novel Ethyl 4-[4-(4-Substitutedpiperidin-1-yl)]benzyl-Phenylpyrrolo[1,2-a]quinoxaline-Carboxylate Derivatives in Myeloid and Lymphoid Leukemia Cell Lines," *Eur. J. Med. Chem.*, 113, pp. 214–227.

[28] Cernak, T., Dykstra, K. D., Tyagarajan, S., Vachal, P., and Krska, S. W., 2016, "The Medicinal Chemist's Toolbox for Late-Stage Functionalization of Drug-Like Molecules," *Chem. Soc. Rev.*, 45(3), pp. 546–576.

[29] Ardenne, M., and Reitnauer, P. G., 1975, "[Demonstration of Tumor Inhibiting Properties of a Strongly Immunostimulating Low-Molecular Weight Substance. Comparative Studies with Ifosfamide on the Immuno-Labile DS Carcinosarcoma. Stimulation of the Autoimmune Activity for Approx. 20 Days by BA 1, a N-(2-Cyanoethylene)-Urea. Novel Prophylactic Possibilities]," *Arzneimittelforschung*, 25(9), pp. 1369–1379.

[30] Smith McWilliams, A. D., *et al.*, 2021, "Understanding the Exfoliation and Dispersion of Hexagonal Boron Nitride Nanosheets by Surfactants: Implications for Antibacterial and Thermally Resistant Coatings," *ACS Appl. Nano Mater.*, 4(1), pp. 142–151.

[31] Sakr, A., Brégeon, F., Mège, J.-L., Rolain, J.-M., and Blin, O., 2018, "*Staphylococcus aureus* Nasal Colonization: An Update on Mechanisms, Epidemiology, Risk Factors, and Subsequent Infections," *Front. Microbiol.*, 9, p. 2419.

[32] Pasta, M., Wessells, C. D., Cui, Y., and La Mantia, F., 2012, "A Desalination Battery," *Nano Lett.*, 12(2), pp. 839–843.